Moisture-vortex instability and the growth of South Asian monsoon low-pressure systems

Ángel F. Adames[1,2] and Yi Ming[1]

[1] *Geophysical Fluid Dynamics Laboratory/NOAA,*

Princeton, NJ

[2] *University Corporation for Atmospheric Research*

Boulder, CO

* *Corresponding author address: 201 Forrestal Rd*

Princetion, NJ, 08536

Email: Angel.Adames-Corraliza@noaa.gov

ABSTRACT

Monsoon low pressure systems, referred to as synoptic-scale monsoonal disturbances (SMDs), are modes of monsoonal variability that have a large influence in rainfall over the South Asian monsoon region. It has long been thought that these systems grow due to moist baroclinic instability, a variant of baroclinic instability that includes the effects of deep convection. Recent work, however, has shown that this framework is inconsistent with the observed structure and dynamics of SMDs.

Here we present an alternative framework where moisture is prognostic and is coupled to precipitation through a simplified Betts-Miller parameterization. Unstable Rossby-like wave solutions are obtained that arise from interactions between moisture, convection and the anomalous circulation in the presence of a background temperature gradient. Warm air that is advected south by the anomalous flow is lifted along the sloping isentropes of the monsoon region, which moistens and destabilizes the column to the west of the low-pressure center. The moistened lower troposphere enhances convection which, in turn, causes the low pressure system to intensify through vortex stretching. It is shown that during the active months of the South Asian monsoon unstable growth occurs only if the moist wave can propagate westward against the low-level westerly flow. For parameter values that resemble the observed monsoonal background state, growth of these waves is largest at the synoptic scale. Expanding the framework to include meridional moisture gradients leads to a more general framework that suggests this "moisture-vortex" instability may operate on other synoptic-scale low pressure systems such as easterly waves.

1. Introduction

Monsoon low pressure systems are synoptic-scale cyclones that occur during the active months of the Indian monsoon. They predominantly develop over the Bay of Bengal, propagate northwestward towards the Indian subcontinent with a phase speed of ~ 5 m s^{-1} (Mooley 1973; Godbole 1977; Krishnamurti and Chow 1975, 1976; Sikka 1977; Hunt and Turner 2017). As they propagate northwestward, they produce a large fraction of the total monsoonal rainfall received by India (Stano et al. 2002; Ding and Sikka 2006; Yoon and Chen 2005; Yoon and Huang 2012). The influence of these synoptic-scale monsoonal disturbances (SMDs) on total monsoon precipitation indicates that understanding the mechanisms by which they propagate and grow is of central importance to our understanding of the Indian monsoon.

It has long been thought that SMDs are destabilized by a variant of baroclinic instability (Charney and Stern 1962; Bretherton 1966) that is modified by diabatic heating, referred to "moist baroclinic instability" (Salvekar et al. 1986; Krishnakumar et al. 1992; Aravequia et al. 1995; de Vries et al. 2010; Krishnamurti et al. 2013). Similarly to the original dry baroclinic instability model, this moist model includes counterpropagating waves that can phase lock and induce mutual growth. For this phase locking to occur, the anomalies in potential vorticity must tilt against the climatological-mean vertical wind shear (de Vries et al. 2010; Cohen and Boos 2016).

However, it was recently shown by Cohen and Boos (2016) that the structure of SMDs, as described by modern reanalysis products, is inconsistent with the criteria necessary for moist baroclinic instability to occur. Furthermore, Boos et al. (2015) found that the quasi-geostrophic (QG) approximation, which is often employed in studies of monsoon low pressure systems (Subrahmanyam et al. 1981; Sanders 1984) may not be adequate for the study of SMDs.

More recently, Adames and Ming (2017) analyzed the moisture and moist static energy budgets of SMDs as simulated in GFDL's atmospheric general circulation model

AM4.0. They found a strong coupling between anomalous precipitation and column moisture anomalies. The moisture anomalies were found to propagate due to horizontal advection of mean dry static energy (DSE) by the anomalous winds. This horizontal advection of DSE induces a moisture tendency by forcing ascent along the sloping isentropes of the monsoon region. This result is inconsistent with the traditional QG assumption of forced ascent being tightly coupled to the precipitation field (Mak 1982; Sanders 1984). Moist processes play a critical role in the simulated SMDs and a prognostic moisture equation may be necessary to fully capture their dynamics.

In this study we propose a linear framework for SMDs which incorporates a prognostic equation for column moisture, akin to the "moisture mode" framework commonly used to study the Madden-Julian Oscillation (MJO) (Raymond and Fuchs 2009; Sobel and Maloney 2012, 2013; Adames and Kim 2016). By incorporating a prognostic equation for column moisture, an instability arises that may describe the growth of SMDs. This instability involves a coupling between lower tropospheric vorticity and column moisture. Warm air advection by the anomalous winds causes moist near-surface air to lift, moistening the free troposphere ahead of the cyclone and creating an environment favorable for deep convection. This subsequent convection intensifies the SMD through vortex stretching. We will show that this mechanism is analogous to meridional moisture advection, and when both warm air and moisture advection are considered together as moist static energy advection, the framework may also be applicable to other moist low-pressure systems such as easterly waves (Lau and Lau 1990, 1992; Kiladis et al. 2006; Serra et al. 2008; Rydbeck and Maloney 2015).

This paper is structured as follows. The next section offers a simple theoretical framework that can describe the structure and growth of SMDs. A thorough discussion of the implications of the framework presented here is offered in Section 3. A few concluding remarks are offered in Section 4.

2. A linear model for SMDs with prognostic moisture

In this section we present a linear theoretical framework that can explain the growth and propagation of SMDs. We will begin by presenting a set basic equations linearized with respect to a background state that resembles the monsoon circulation. This includes mean low-level westerly winds and a horizontal temperature distribution that increases with latitude. The field variables are thus separated into time-mean (denoted by an overbar) and perturbation (denoted by a prime) components. The nomenclature used here closely follows the so-called moisture mode treatments of the MJO (Sobel and Maloney 2012, 2013; Adames and Kim 2016). The most important variables and definitions used in this section are summarized in Table 1.

It was found by Hunt et al. (2016) that precipitation in SMDs is colocated with enhanced convective available potential energy (CAPE). They found that the enhanced CAPE is due to increased lower tropospheric (elevated boundary layer and lower free troposphere) moisture elevating the equivalent potential temperature of rising parcels. Similarly, Adames and Ming (2017) found that column moisture and precipitation are highly correlated in space in SMDs simulated by GFDL's atmospheric general circulation model (AM4.0). We can thus parameterize anomalous precipitation as a function of anomalous column water vapor $\langle q' \rangle$ using a simplified Betts-Miller scheme (Betts and Miller 1986; Betts 1986; Frierson 2007)

$$P' = \frac{\langle q' \rangle}{\tau_c} \tag{1}$$

where angle brackets denote vertical mass-weighted integration from 100 to 1000 hPa. Note that, following Neelin and Zeng (2000) and Adames and Kim (2016), q and P will be implicitly scaled by the latent energy of vaporization L_v. With the above approximation, the leading terms in the momentum, thermodynamic and column-integrated moisture equations are written as follows

$$\frac{\partial u'}{\partial t} = -\overline{u}_0 \frac{\partial u'}{\partial x} + f v' - \frac{\partial \phi'}{\partial x} \tag{2a}$$

$$\frac{\partial v'}{\partial t} = -\overline{u}_0 \frac{\partial v'}{\partial x} - f u' - \frac{\partial \phi'}{\partial y} \tag{2b}$$

$$-\overline{M_s}D' = P' - v'\frac{\overline{M_s}\beta_T}{f_0} \tag{2c}$$

$$\frac{\partial P'}{\partial t} = -\frac{1}{\tau_c}\left(\overline{M_q}D' + P'\right) \tag{2d}$$

where u' and v' are the zonal and meridional wind anomalies, respectively, $\overline{u_0}$ is the climatological-mean barotropic flow, $f = f_0 + \beta y$ is the linearized planetary vorticity and $D' = \nabla \cdot \mathbf{v}'$ is the anomalous lower-tropospheric horizontal divergence. $\overline{M_q} = \langle \Omega \partial \overline{q}/\partial p \rangle$ and $\overline{M_s} = -\langle \Omega \partial \overline{S}/\partial p \rangle$ are the gross moisture stratification and the gross dry stability, respectively, and their definitions are as in Neelin and Zeng (2000) and Adames and Kim (2016), where Ω is the vertical structure of ascent and $\overline{S}$ is the dry static energy (see Appendix). β_T is the climatological-mean meridional temperature gradient, scaled so that it is in the same units as β

$$\beta_T = \frac{f_0 C_p}{\overline{M_s}}\left\langle \Lambda \frac{\partial \overline{T}}{\partial y} \right\rangle \tag{3}$$

where C_p is the specific heat of dry air, Λ is the vertical structure function of the horizontal winds (see Adames and Kim 2016 for definitions and values). It can be shown that β_T is related to the mean vertical wind shear through the thermal wind equation

$$\beta_T = \frac{f_0^2 C_p}{R_d \overline{M_s}}\left\langle \Lambda \frac{\partial \overline{u}}{\partial \ln p} \right\rangle \tag{4}$$

where R_d is the dry gas constant and $\overline{u}$ is the total mean zonal wind. We have defined our variables such that the vertical structure functions Ω and Λ are contained within β_T, $\overline{M_s}$ and $\overline{M_q}$. It is possible that variations in these variables arise from those of the mean state and from variations in the vertical structure of the wave.

The terms in the right-hand side of Eqs. (2a) and (2b) are advection of the winds by the layer-mean (barotropic) flow, the Coriolis acceleration and the pressure gradient force, respectively. The terms on the right hand side of Eq. (2c) correspond to diabatic heating by convection and meridional temperature advection, respectively. Note that this equation suggests that there are two contributions to divergence, a convectively-driven one $D'_c = P'/\overline{M_s}$ and an advectively-driven component $D'_a = v'\beta_T/f_0$. Note that in this framework, D'_a describes ascent along sloping isentropes. Finally, the equation for column moisture, which is converted to a precipitation equation via Eq. (1), contains two terms on the right hand side: the contribution of vertical moisture advection and the loss of moisture through precipitation.

We can differentiate Eqs. (2a) and (2b) with respect to y and x, respectively, and convert them into a perturbation vorticity equation

$$\frac{\partial \zeta'}{\partial t} = -\overline{u_0}\frac{\partial \zeta'}{\partial x} - v'\beta - f_0 D' \tag{5}$$

The right-hand side terms of Eq. (5) correspond to advection of anomalous vorticity by the mean winds, advection of absolute vorticity by the anomalous meridional flow, and generation of vorticity by anomalous divergence (Sardeshmukh and Hoskins 1988). We can remove D' from the equations by merging Eqs. (2c) and (5), and similarly Eqs. (2c) and (2d), which leads us to the following two equations

$$\frac{\partial \zeta'}{\partial t} = -\overline{u_0}\frac{\partial \zeta'}{\partial x} - v'(\beta + \beta_T) + \frac{f_0}{\overline{M_s}}P' \tag{6a}$$

$$\frac{\partial P'}{\partial t} = -\frac{1}{\tau_c}\left(\tilde{M}P' + \overline{M_q}v'\frac{\beta_T}{f_0}\right) \tag{6b}$$

where $\tilde{M} = (\overline{M_s} - \overline{M_q})/\overline{M_s}$ is the normalized gross moist stability (NGMS), a measure of the effective static stability of the atmosphere. Two terms contribute to the evolution of moisture. The first term on the right hand side describes the effect deep convection on moisture. For values of $\tilde{M} > 0$, the loss of moisture through condensation exceeds the supply of it through convectively-driven ascent, thus damping the wave. The second term corresponds to the vertical advection of moisture that is induced by horizontal temperature advection, and can be thought of as the adiabatic contribution to the moisture tendency.

In order to further simplify the equations, we will assume that the winds are approximately non-divergent, and thus can be expressed in terms of a streamfunction

$$\zeta' = -\nabla^2\psi' \tag{7a}$$

$$v' \simeq \frac{\partial \psi'}{\partial x} \tag{7b}$$

Substituting ζ' and v' in Eqs. (6a) and (6b) with Eqs. (7a) and (7b) reduces our set of variables to two. Thus, we can now solve our system of equations by assuming that it has a solution in the form of a wave

$$\psi'(x,y,t) = \psi'_0 \exp(ikx + ily - i\omega t) \tag{8a}$$

$$P'(x,y,t) = P'_0 \exp(ikx + ily - i\omega t) \tag{8b}$$

We can substitute Eqs. (8a) and (8b) onto Eqs. (6a) and (6b) and obtain the following dispersion relation:

$$-\omega + \overline{u_0}k - \frac{k}{k^2+l^2}\left(\beta + \beta_T \frac{1 - i\omega\tau_c}{\tilde{M} - i\omega\tau_c}\right) = 0 \tag{9}$$

The two solutions that arise from this dispersion relation are shown in Fig. 1 for a mean zonal flow of 5 m s^{-1}, meridional wavenumber 15, $\tilde{M} = 0.15$ and $\beta_T = 0.75 \times 10^{-11}$ m^{-1} s^{-1}. The value of β_T is chosen so that it approximately corresponds to a lower-tropospheric temperature gradient of 1.5°C per 1000 km. The meridional wavenumber chosen so that it qualitatively represents the meridional extent of the region of westerly winds in the south Asian monsoon. The solutions are reminiscent of a pair of Rossby waves, one eastward-propagating and one westward-propagating. For positive NGMS and small τ_c, the eastward-propagating solution is strongly damped (damping is beyond the edges in the top panel of Fig. 1) while the westward-propagating solution is unstable within zonal wavenumbers 1-20.

Further insight of the growing solution in Fig. 1 can be obtained by making the approximation that $\tilde{M}^2 \gg \tau_c^2\omega^2$, which can be shown to be a reasonable approximation for values of τ_c of roughly an hour and values of $\tilde{M} \simeq 0.15$. This may not be fully realistic, but it simplifies our solutions substantially and allows for some important insights that are still valid for larger values of τ_c [Adames and Ming (2017) found $\tau_c \sim 4.5$ hours in simulated depressions]. With this approximation, the dispersion relation takes the following form:

$$-\omega + \overline{u_0}k - \frac{k}{k^2+l^2}\left(\beta + \frac{\beta_T}{\tilde{M}} - \frac{i\omega\beta_T\tau_c\left(1-\tilde{M}\right)}{\tilde{M}^2}\right) \simeq 0 \tag{10}$$

In order to simplify our calculations, we define the following

$$c_p^x = \overline{u_0} - \frac{1}{k^2+l^2}\left(\beta + \frac{\beta_T}{\tilde{M}}\right) \tag{11}$$

which will be shown later to correspond to the approximate phase speed of the wave. This phase speed describes a Rossby wave that is augmented by a contribution from $\beta_T/\tilde{M}$. This contribution arises from meridional temperature advection augmented by vortex stretching from precipitation. Following Cohen and Boos (2016), we can describe this phase speed as a combination of a dry component due to vorticity advection and adiabatic ascent driven by horizontal temperature advection, and a moist component due to vortex stretching from deep convection:

$$c_p^x = c_{pd}^x + c_{pm}^x \tag{12a}$$

$$c_{pd}^x = \overline{u_0} - \frac{\beta + \beta_T}{k^2+l^2} \tag{12b}$$

$$c_{pm}^x = -\frac{\beta_T(1-\tilde{M})}{\tilde{M}(k^2+l^2)} \tag{12c}$$

By using these definitions, Eq. (10) can be simplified to the following

$$\omega\left(\tilde{M} - i\tau_c c_{pm}^x k\right) \simeq \tilde{M} c_p^x k \tag{13}$$

We can once again approximate $\tilde{M}^2 \gg \tau_c^2\omega^2$ (or more specifically $\tilde{M}^2 \gg \tau_c^2 c_{pm}^2 k^2$), with little loss of accuracy (not shown). With this approximation, we obtain Eq. (11) as our zonal phase speed and the approximate zonal group velocity is of the form

$$c_g^x \simeq \overline{u_0} + \frac{(k^2-l^2)}{(k^2+l^2)^2}\left(\beta + \frac{\beta_T}{\tilde{M}}\right) \tag{14}$$

and the growth rate of the low pressure system is

$$\mathrm{Im}(\omega) \simeq \frac{\tau_c k^2}{\tilde{M}} c_{pm}^x c_p^x \tag{15}$$

which indicates that the wave is unstable as long as c_p^x and c_{pm}^x are in the same direction. In the case of monsoon low pressure systems analyzed here, both c_p^x and c_{pm}^x are required to be westward for the disturbance to grow, which implies that growing depressions propagate against the mean westerly flow. By finding the zonal wavenumber k_{max} which satisfies $\partial \mathrm{Im}(\omega)/\partial k = 0$, we can show that growth is a maximum when the following criteria is satisfied

$$c^x_{pm} c^x_g + c^x_{gm} c^x_p = 0 \tag{16}$$

where c^x_{gm} is the moist component of the group velocity

$$c^x_g = \frac{(k^2 - l^2)}{(k^2 + l^2)^2} \frac{\beta_T}{\tilde{M}} (1 - \tilde{M}) \tag{17}$$

which, for $\overline{u_0} = 0$, yields $k_{max} = l$, which implies that the fastest growing modes are characterized by a zero group velocity $c_{gm} = c_g = 0$. Furthermore $k_{max} < l$ for mean westerly flow, $k_{max} > l$ for easterly flow (not shown).

The red line in Fig. 1 shows the phase speed and growth rate obtained from Eqs. (11) and (15). The solution is nearly indistinguishable from the westward-propagating solution of Eq. (9) for a value of τ_c of one hour. For a value of τ_c similar to that found by Adames and Ming (2017), the approximate solution overestimates the phase speed and the growth rate, but is still able to qualitatively capture the shape of the dispersion curves, with the maxima and nodes occurring over the same zonal wavenumbers. To further understand our wave solution, Fig. 2 shows the approximate zonal phase speed, group velocity and growth rate of the linear solutions for values of β_T ranging from 0 to $1{\times}10^{-11}$ m^{-1} s^{-1}. When $\beta_T = 0$, which results in a dry Rossby wave, the wave is neutrally stable and unable to propagate against the mean zonal flow. As β_T increases, more zonal wavenumbers are able to propagate against the mean zonal flow while exhibiting unstable growth. Stronger growth occurs for larger values of β_T, and the maximum growth is observed near zonal wavenumber 10, consistent with the synoptic scale of monsoon low pressure systems. Thus, the instability that is describe in these linear wave solutions may be able to describe the observed scale of SMDs.

Some insight of the physical mechanism that leads to the growth in Eq. (15) may be obtained by looking at horizontal maps of the corresponding linear solutions, shown in Fig.

3. For these panels we use a value of τ_c of 18 hours. While this value is too large for the approximations done in the previous sections, it reveals the phasing between the fields more clearly than using a value of several hours. The top panel shows a wave solution in which c_p^x and c_{pm}^x propagate westward. This case is analogous to a monsoon low pressure system propagating westward in an environment characterized by mean westerly winds and a positive meridional temperature gradient. In such a case, anomalous northerly flow induces isentropic ascent, which moistens the troposphere, resulting in a positive precipitation tendency, as shown in Fig. 4a. The increasing precipitation removes moisture from the column, offsetting the moistening from isentropic ascent. The sum of the two processes results in westward propagation of the anomalous precipitation region.

As the wave propagates westward, precipitation increases and reaches a maximum amplitude at a time when the the cyclonic anomalies exhibit an in-phase component with enhanced precipitation. This in-phase component of precipitation generates additional cyclonic vorticity (Eq. 6a), which causes the cyclonic anomalies to grow. It is also noteworthy that the interaction between isentropic ascent and deep convective ascent causes vertical motion (convergence) to slightly lead precipitation, as shown in panels (b) and (c) of Fig. 4. This phasing between vertical motion and precipitation was found in simulated monsoon depressions by Adames and Ming (2017).

When c_p^x and c_{pm}^x are in opposite directions, as shown in the bottom panel of Fig. 3, anomalous northerly flow still induces a precipitation tendency. However, because the wave is propagating in the opposite direction as c_{pm}^x, precipitation reaches a maximum amplitude with a component that is in-phase with the anticyclonic anomalies. Because precipitation generates a cyclonic tendency, it follows that it will damp the anticyclonic anomalies.

3. Synthesis

In this study we presented a linear framework that may explain the propagation and growth of SMDs. Based on results from recent observational and modeling studies (Hunt et al. 2016; Adames and Ming 2017), we propose that column moisture plays a central role in SMDs. By including a prognostic moisture equation and coupling it to precipitation through a simplified Betts-Miller scheme, we derive a dispersion describes the following features of SMDs, including:

- their synoptic scale (wavelength of 2000-3000 km)
- westward propagation against the mean westerly flow.

In addition to these feautures, it describes a new instability mechanism that may explain the growth of these disturbances. This instability only occurs if the wave's dry and moist phase speeds are in the same direction. The dry phase speed includes dry processes such as advection of planetary vorticity by the anomalous winds, advection of anomalous vorticity by the mean flow and vortex stretching from isentropic ascent. The moist phase speed only includes propagation that is induced by vortex stretching from deep convection. The instability is a result of isentropic ascent moistening the free troposphere, producing an environment conducive for deep convection, as shown schematically in Fig. 5. This subsequent convection occurs in-phase with the cyclonic anomalies, which intensifies them through vortex stretching. This result implies that, in the South Asian monsoon region, where the temperature gradient is positive and the mean flow westerly, only SMDs that can propagate westward against the mean flow can grow.

a. Comparison to baroclinic instability

Previous studies have sought to describe SMDs as a result of moist baroclinic instability (Charney and Stern 1962; Bretherton 1966) which relies on the existence of counterpropagating waves for their growth (Sanders 1984; Snyder and Lindzen 1991). Unlike existing models of moist baroclinic instability (de Vries et al. 2010, see review by Cohen and Boos 2016), the framework presented here only involves dry and moist waves in the lower troposphere propagating in the same direction. The middle and upper troposphere do not play a role in the instability of SMDs.

Furthermore, most studies that involve the use of baroclinic instability diagnose convection from the QG omega equation. In the QG framework, ascent occurs in regions of warm air advection, which is related to the geostrophic thermal wind [Eq. (1) in Boos et al. 2015] as follows

$$P' \propto v' \frac{\partial u_g}{\partial p} \tag{18}$$

For a mean state in geostrophic balance $\overline{u} = u_g$, it can be shown that QG ascent is proportional to lifting occuring over sloping isentropes D'_a. Using this parameterization, where moisture is not prognostic, yields solutions similar to those shown in Section 2, but the solutions are neutrally stable.

In the framework presented here, convection is parameterized in terms of column water vapor. By doing this, isentropic ascent is not just associated with convection, but to a positive moisture tendency, as seen in Eq. (6b) and Fig. 4. Such a relationship was found by Adames and Ming (2017), suggesting that moisture may play a critical role in the growth of SMDs.

b. Comparison to the balanced moisture waves of Sobel et al. (2001)

While the framework presented here differs significantly from models of moist baroclinic instability, it resembles the balanced moisture waves described by Sobel et al. (2001) (see their Eqs. 42 and 45). The main difference between the solutions shown here and theirs is the presence of a temperature gradient instead of a moisture gradient. This implies that the low-frequency background is not in weak temperature gradient balance, a deviation that arises from the land-sea contrast over the South Asian monsoon region. Even though the background does not satisfy WTG balance, the temperature anomalies are not included in the wave solution, and thus an analysis similar to the one employed in WTG balance studies (see for example Chikira 2014; Wolding and Maloney 2015) can be applied here. This simplification is justifiable since Adames and Ming (2017) found that the column-integrated temperature tendency is negligibly small compared to the contribution from apparent heating.

We can show that the solutions of Sobel et al. (2001) are similar to the ones derived here. If we add a meridional mean moisture gradient of the form $\beta_q = f_0 L_v \overline{M_q}^{-1} \langle \Lambda \partial_y \overline{q} \rangle$, as in Sobel et al. (2001) but scaled so that it is in units of $m^{-1}s^{-1}$, to Eq. (2d), the following approximate solution for c^x_{pm} may be obtained for sufficiently small values of $\tilde{M}$:

$$c^x_{pm} = -\frac{\beta_h(1-\tilde{M})}{\tilde{M}(k^2+l^2)} \tag{19}$$

where $\beta_h = \beta_T + \beta_q$. Note that c^x_{pd} does not change with this addition. Thus, the moisture and temperature gradients behave in analogous ways in this framework. When the linear solution presented here is merged with those of Sobel et al. (2001) they can be expressed in terms of a moist static energy (MSE) "beta plane."

c. *Relevance to other tropical depression disturbances*

The dispersion relation derived here and its generalization described in the previous subsection may shed some insight onto other tropical depression disturbances beyond the Indian monsoon region. For example, Kiladis et al. (2006) found that divergence of the Q-vectors (which is related to β_T) leads convection by 1/8 cycle. Furthermore, Rydbeck and Maloney (2015) and Rydbeck et al. (2017) analyzed easterly waves occuring over the tropical northeastern Pacific. They found that when the waves are developing, meridional moisture advection and vortex stretching play a key role the growth and propagation of these waves. The framework used here may provide insights into the dynamics of easterly waves over

African and the eastern Pacific. It is possible that is also relevant in other regions where Rossby-like low pressure systems form (see Hurley and Boos 2015).

d. Comparison with "moisture mode" theory of the MJO

It is worth comparing the moist waves described here to the linear "moisture mode" theory of the MJO (Fuchs and Raymond 2005; Sobel and Maloney 2012, 2013; Adames and Kim 2016). In the moisture mode framework, propagation of the wave is induced by processes that modulate the distribution of column-integrated moisture. Its growth rate is negatively related to the NGMS and inversely proportional to τ_c. In the moist waves presented here, the relationships between NGMS, τ_c and growth are inverse to those in MJO moisture mode theory. This difference is due to the way that moisture interacts with the anomalies in both frameworks. In the framework presented here, propagation and growth is partly due to the impact of moisture-convection feedbacks on the vorticity (wind) field. In the MJO, propagation is due to the modulation of moisture by the wind anomalies.

This result implies that the existence of a prognostic moisture equation can cause instability through different mechanisms. In the MJO the process has been referred to as "moisture mode" instability, or simply moisture instability. The instability for the moist Rossby-like waves presented may also be interpreted as a different type of moisture instability, but related to the impact moisture has on vorticity. Thus, it may be more appropriate to refer to this instability as "moisture-vortex" instability. That the interaction between moisture and the large-scale flow can lead to more than one instability is interesting, and their manifestation in observations is worth exploring in the future.

4. Concluding remarks

We have not discussed to this point the meridional propagation of SMDs. For the plots shown here, we used a meridionally-decaying structure, which is roughly consistent with the observed structure of these waves. However, we did not discuss the meridional propagation of westward-propagating SMDs. Observed depression systems exhibit a northward component to propagation (Krishnamurthy and Ajayamohan 2010; Cohen and Boos 2016). Further work could more clearly shed light on how the monsoonal mean state shapes the meridional structure of monsoon low pressure systems.

It was recently shown by Boos et al. (2015) that nonlinear horizontal vorticity advection plays a central role in the northwestward propagation of monsoon low pressure systems. This mechanism was not included due to the linear nature of the analysis shown here. It would be interesting to see how the so-called beta drift interacts with moisture within this context. It would also be interesting to see whether an analysis like the one done by Cohen and Boos (2016) for developing depressions supports the instability mechanism proposed here. Additionally, a mean state with positive-only precipitation is assumed, which may be an oversimplification of the monsoonal mean state.

The vertical structure of the wave is treated as being directly related to the profile of vertical motion, which is in turn related to deep convection. As a result, the waves discussed here approximately have a first baroclinic vertical structure. Observed monsoon low pressure systems, however, exhibit a vertical structure that is closer to barotropic. Such a discrepancy is a caveat of this study. Nonetheless, the linear framework presented here presents an intriguing interpretation of monsoon low pressure systems which can be tested in model simulations. For example, simulations in which moisture is treated diagnostically may produce weaker disturbances than those that treat moisture prognostically, as suggested by the growth rate in Eq. (15). These and other studies are interesting directions for future study.

Acknowledgments. This work was supported by the National Oceanic and Atmospheric Administration (NOAA) grant NA15OAR4310099. We would like to thank Eric Maloney for conversations that motivated some of the discussion presented here. We would also like to thank Kuniaki Inoue and Nadir Jeevanjee for comments that helped improve the manuscript.

APPENDIX

Vertical truncation of the equations

In this section we describe the vertical truncation of the equations shown in Section 2. The method is identical to that of Adames and Kim (2016), but is included here for clarity. Following Neelin and Zeng (2000), we separate the vertical velocity field into a horizontal divergence field D and a structure function Ω that describes the profile of vertical velocity ω (note that in Section 3 ω corresponds to the wave frequency instead)

$$\omega(x, y, p, t) = D(x, y, t)\Omega(p) \tag{A1}$$

where we make use of a single vertical structure function that corresponds to deep convection (a first baroclinic mode in vertical motion). Following a rigid lid boundary condition, Ω must be equal to zero at 1000 hPa and 100 hPa. We use a simple formula for Ω that satisfies these conditions, which is similar to the formulas used by Haertel et al. (2008) and Kiladis et al. (2009)

$$\Omega(p) = \hat{p}\,(p/p_s)^{-1/2}\sin(mp - \theta_p) \tag{A2}$$

where $\hat{p} = 80$ hPa is a reference value for vertical velocity, $p_s = 1000$ hPa is the surface pressure, $m = 2\pi/p_\lambda$ is the vertical wavenumber, $p_\lambda = 1800$ hPa is the vertical wavelength, and $\theta_p = 2\pi/p_b$ is a phase shift angle, where $p_b = 18$ hPa. A similar profile to this can be obtained from EOF analysis of vertical velocity along the equatorial belt (see Fig. 6 of Adames and Wallace 2014).

Similarly, the horizontal wind field $\mathbf{V} = (U, V)$ and geopotential Φ are separated into a horizontal component and a vertical structure function

$$\mathbf{V}(x, y, p, t) = \mathbf{v}(x, y, t)\Lambda(p) \tag{A3a}$$

$$\Phi(x, y, p, t) = \phi(x, y, t)\Lambda(p) \tag{A3b}$$

where $\mathbf{v} = (u, v)$ and the structure function Λ is obtained from Ω through mass continuity:

$$\Lambda(p) = -\frac{\partial \Omega(p)}{\partial p} \tag{A4}$$

Using this truncation of the vertical structure functions and with vertical mass integration, we can rewrite the terms involving meridional temperature advection, vertical DSE advection vertical moisture advection as follows

$$\left\langle V' \frac{\partial \overline{T}}{\partial y} \right\rangle = v' \left\langle \Lambda \frac{\partial \overline{T}}{\partial y} \right\rangle \tag{A5a}$$

$$\left\langle \omega' \frac{\partial \overline{S}}{\partial p} \right\rangle = D' \left\langle \Omega \frac{\partial \overline{S}}{\partial p} \right\rangle \tag{A5b}$$

$$\left\langle \omega' \frac{\partial \overline{q}}{\partial p} \right\rangle = D' \left\langle \Omega \frac{\partial \overline{q}}{\partial p} \right\rangle \tag{A5c}$$

and through rearrangement of the terms we can define β_T, $\overline{M_s}$ and $\overline{M_q}$ to obtain the corresponding terms in Eq. (2c) and (2d).

REFERENCES

Adames, Á. F., and D. Kim, 2016: The MJO as a Dispersive, Convectively Coupled Moisture Wave: Theory and Observations. *J. Atmos. Sci.*, **73 (3)**, 913–941.

Adames, A. F., and Y. Ming, 2017: Moisture and moist static energy budgets of monsoon depressions in GFDL AM4. *J. Atmos. Sci.*

Adames, Á. F., and J. M. Wallace, 2014: Three-Dimensional Structure and Evolution of the Vertical Velocity and Divergence Fields in the MJO. *J. Atmos. Sci.*, **71 (12)**, 4661–4681.

Aravequia, J. A., V. B. Rao, and J. P. Bonatti, 1995: The role of moist baroclinic instability in the growth and structure of monsoon depressions. *Journal of the Atmospheric*

Sciences, **52 (24)**, 4393–4409, doi:10.1175/1520-0469(1995)052⟨4393:TROMBI⟩2.0.CO;2, URL https://doi.org/10.1175/1520-0469(1995)052⟨4393:TROMBI⟩2.0.CO;2, https://doi.org/10.1175/1520-0469(1995)052⟨4393:TROMBI⟩2.0.CO;2.

Betts, A., and M. Miller, 1986: A new convective adjustment scheme. Part II: Single column tests using GATE wave, BOMEX, ATEX and arctic air-mass data sets. *Quarterly Journal of the Royal Meteorological Society*, **112 (473)**, 693–709.

Betts, A. K., 1986: A new convective adjustment scheme. Part I: Observational and theoretical basis. *Quarterly Journal of the Royal Meteorological Society*, **112 (473)**, 677–691.

Boos, W. R., J. V. Hurley, and V. S. Murthy, 2015: Adiabatic westward drift of indian monsoon depressions. *Quarterly Journal of the Royal Meteorological Society*, **141 (689)**, 1035–1048, doi:10.1002/qj.2454, URL http://dx.doi.org/10.1002/qj.2454.

Bretherton, F. P., 1966: Baroclinic instability and the short wavelength cut-off in terms of potential vorticity. *Quarterly Journal of the Royal Meteorological Society*, **92 (393)**, 335–345, doi:10.1002/qj.49709239303, URL http://dx.doi.org/10.1002/qj.49709239303.

Charney, J. G., and M. E. Stern, 1962: On the stability of internal baroclinic jets in a rotating atmosphere. *Journal of the Atmospheric Sciences*, **19 (2)**, 159–172, doi:10.1175/1520-0469(1962)019⟨0159:OTSOIB⟩2.0.CO;2, URL https://doi.org/10.1175/1520-0469(1962)019⟨0159:OTSOIB⟩2.0.CO;2, https://doi.org/10.1175/1520-0469(1962)019⟨0159:OTSOIB⟩2.0.CO;2.

Chikira, M., 2014: Eastward-propagating intraseasonal oscillation represented by Chikira–Sugiyama cumulus parameterization. Part II: Understanding moisture variation under weak temperature gradient balance. *J. Atmos. Sci.*, **71 (2)**, 615–639.

Cohen, N. Y., and W. R. Boos, 2016: Perspectives on moist baroclinic instability: Implications for the growth of monsoon depressions. *Journal of the Atmospheric Sci-*

ences, **73 (4)**, 1767–1788, doi:10.1175/JAS-D-15-0254.1, URL http://dx.doi.org/10.1175/JAS-D-15-0254.1, http://dx.doi.org/10.1175/JAS-D-15-0254.1.

de Vries, H., J. Methven, T. H. A. Frame, and B. J. Hoskins, 2010: Baroclinic waves with parameterized effects of moisture interpreted using rossby wave components. *Journal of the Atmospheric Sciences*, **67 (9)**, 2766–2784, doi:10.1175/2010JAS3410.1, URL https://doi.org/10.1175/2010JAS3410.1, https://doi.org/10.1175/2010JAS3410.1.

Ding, Y., and D. R. Sikka, 2006: *Synoptic systems and weather*, 131–201. Springer Berlin Heidelberg, Berlin, Heidelberg, doi:10.1007/3-540-37722-0_4, URL http://dx.doi.org/10.1007/3-540-37722-0_4.

Frierson, D. M. W., 2007: The dynamics of idealized convection schemes and their effect on the zonally averaged tropical circulation. *Journal of the Atmospheric Sciences*, **64 (6)**, 1959–1976, doi:10.1175/JAS3935.1, URL http://dx.doi.org/10.1175/JAS3935.1, http://dx.doi.org/10.1175/JAS3935.1.

Fuchs, Z., and D. J. Raymond, 2005: Large-scale modes in a rotating atmosphere with radiative-convective instability and WISHE. *J. Atmos. Sci.*, **62 (11)**, 4084–4094.

Godbole, R. V., 1977: The composite structure of the monsoon depression. *Tellus*, **29 (1)**, 25–40, doi:10.1111/j.2153-3490.1977.tb00706.x, URL http://dx.doi.org/10.1111/j.2153-3490.1977.tb00706.x.

Haertel, P. T., G. N. Kiladis, A. Denno, and T. M. Rickenbach, 2008: Vertical-Mode Decompositions of 2-Day Waves and the Madden–Julian Oscillation. *J. Atmos. Sci.*, **65 (3)**, 813–833.

Hunt, K. M., and A. G. Turner, 2017: The effect of horizontal resolution on indian monsoon depressions in the met office nwp model. *Quarterly Journal of the Royal Meteorological Society*, **143 (705)**, 1756–1771, doi:10.1002/qj.3030, URL http://dx.doi.org/10.1002/qj.3030.

Hunt, K. M. R., A. G. Turner, P. M. Inness, D. E. Parker, and R. C. Levine, 2016: On the structure and dynamics of indian monsoon depressions. *Monthly Weather Review*, **144 (9)**, 3391–3416, doi:10.1175/MWR-D-15-0138.1, URL http://dx.doi.org/10.1175/MWR-D-15-0138.1, http://dx.doi.org/10.1175/MWR-D-15-0138.1.

Hurley, J. V., and W. R. Boos, 2015: A global climatology of monsoon low-pressure systems. *Quarterly Journal of the Royal Meteorological Society*, **141 (689)**, 1049–1064, doi:10.1002/qj.2447, URL http://dx.doi.org/10.1002/qj.2447.

Janiga, M. A., and C. Zhang, 2016: Mjo moisture budget during dynamo in a cloud-resolving model. *J. Atmos. Sci.*, **73 (6)**, 2257–2278, doi:10.1175/JAS-D-14-0379.1.

Kiladis, G. N., C. D. Thorncroft, and N. M. J. Hall, 2006: Three-Dimensional Structure and Dynamics of African Easterly Waves. Part I: Observations. *Journal of the Atmospheric Sciences*, **63 (9)**, 2212–2230, doi:10.1175/JAS3741.1, URL https://doi.org/10.1175/JAS3741.1, https://doi.org/10.1175/JAS3741.1.

Kiladis, G. N., M. C. Wheeler, P. T. Haertel, K. H. Straub, and P. E. Roundy, 2009: Convectively Coupled Equatorial Waves. *Rev. Geophys.*, 1–42.

Krishnakumar, V., R. N. Keshavamurty, and S. V. Kasture, 1992: Moist baroclinic instability and the growth of monsoon depressions— linear and nonlinear studies. *Proceedings of the Indian Academy of Sciences - Earth and Planetary Sciences*, **101 (2)**, 123–152, doi:10.1007/BF02840349, URL http://dx.doi.org/10.1007/BF02840349.

Krishnamurthy, V., and R. S. Ajayamohan, 2010: Composite structure of monsoon low pressure systems and its relation to indian rainfall. *Journal of Climate*, **23 (16)**, 4285–4305, doi:10.1175/2010JCLI2953.1, URL http://dx.doi.org/10.1175/2010JCLI2953.1, http://dx.doi.org/10.1175/2010JCLI2953.1.

Krishnamurti, K. M. G. R. C. C.-B. C. F., T.-N., and J. H. Chow, 1975: Study of a monsoon depression (I): synoptic structure. *J. Meteorol. Soc. Japan*, **53**, 227–239, doi:10.1175/JAS3741.1.

Krishnamurti, K. M. G. R. C. C.-B. C. F., T.-N., and J. H. Chow, 1976: Study of a monsoon depression (II): dynamical structure. *J. Meteorol. Soc. Japan*, **54**, 208–226, doi:10.1175/JAS3741.1.

Krishnamurti, T. N., A. Martin, R. Krishnamurti, A. Simon, A. Thomas, and V. Kumar, 2013: Impacts of enhanced ccn on the organization of convection and recent reduced counts of monsoon depressions. *Climate Dynamics*, **41 (1)**, 117–134, doi:10.1007/s00382-012-1638-z, URL http://dx.doi.org/10.1007/s00382-012-1638-z.

Lau, K.-H., and N.-C. Lau, 1990: Observed structure and propagation characteristics of tropical summertime synoptic scale disturbances. *Monthly Weather Review*, **118 (9)**, 1888–1913, doi:10.1175/1520-0493(1990)118⟨1888:OSAPCO⟩2.0.CO;2, URL https://doi.org/10.1175/1520-0493(1990)118⟨1888:OSAPCO⟩2.0.CO;2, https://doi.org/10.1175/1520-0493(1990)118⟨1888:OSAPCO⟩2.0.CO;2.

Lau, K.-H., and N.-C. Lau, 1992: The energetics and propagation dynamics of tropical summertime synoptic-scale disturbances. *Monthly Weather Review*, **120 (11)**, 2523–2539, doi:10.1175/1520-0493(1992)120⟨2523:TEAPDO⟩2.0.CO;2, URL https://doi.org/10.1175/1520-0493(1992)120⟨2523:TEAPDO⟩2.0.CO;2, https://doi.org/10.1175/1520-0493(1992)120⟨2523:TEAPDO⟩2.0.CO;2.

Mak, M., 1982: On Moist Quasi-Geostrophic Baroclinic Instability. *Journal of the Atmospheric Sciences*, **39 (9)**, 2028–2037, doi:10.1175/1520-0469(1982)039⟨2028:OMQGBI⟩2.0.CO;2, URL https://doi.org/10.1175/1520-0469(1982)039⟨2028:OMQGBI⟩2.0.CO;2, https://doi.org/10.1175/1520-0469(1982)039⟨2028:OMQGBI⟩2.0.CO;2.

Mooley, D. A., 1973: Some aspects of indian monsoon depressions and the associated rainfall. *Monthly Weather Review*, **101 (3)**, 271–280, doi:10.1175/1520-0493(1973)101⟨0271:

SAOIMD⟩2.3.CO;2, URL https://doi.org/10.1175/1520-0493(1973)101⟨0271:SAOIMD⟩2.3.CO;2, https://doi.org/10.1175/1520-0493(1973)101⟨0271:SAOIMD⟩2.3.CO;2.

Neelin, J. D., and N. Zeng, 2000: A Quasi-Equilibrium Tropical Circulation Model—Formulation*. *J. Atmos. Sci.*, **57 (11)**, 1741–1766.

Raymond, D. J., and Ž. Fuchs, 2009: Moisture Modes and the Madden–Julian Oscillation. *J. Climate*, **22 (11)**, 3031–3046.

Rydbeck, A. V., and E. D. Maloney, 2015: On the convective coupling and moisture organization of east pacific easterly waves. *Journal of the Atmospheric Sciences*, **72 (10)**, 3850–3870, doi:10.1175/JAS-D-15-0056.1, URL https://doi.org/10.1175/JAS-D-15-0056.1, https://doi.org/10.1175/JAS-D-15-0056.1.

Rydbeck, A. V., E. D. Maloney, and G. J. A. Jr., 2017: In situ initiation of east pacific easterly waves in a regional model. *Journal of the Atmospheric Sciences*, **74 (2)**, 333–351, doi:10.1175/JAS-D-16-0124.1, URL https://doi.org/10.1175/JAS-D-16-0124.1, https://doi.org/10.1175/JAS-D-16-0124.1.

Salvekar, P. S., L. George, and S. K. Mishra, 1986: Low level wind shear and baroclinic growth of monsoon depression scale waves. *Meteorology and Atmospheric Physics*, **35 (1)**, 10–18, doi:10.1007/BF01029520, URL http://dx.doi.org/10.1007/BF01029520.

Sanders, F., 1984: Quasi-geostrophic diagnosis of the monsoon depression of 5-8 july 1979. *Journal of the Atmospheric Sciences*, **41 (4)**, 538–552, doi:10.1175/1520-0469(1984)041⟨0538:QGDOTM⟩2.0.CO;2, URL https://doi.org/10.1175/1520-0469(1984)041⟨0538:QGDOTM⟩2.0.CO;2, https://doi.org/10.1175/1520-0469(1984)041⟨0538:QGDOTM⟩2.0.CO;2.

Sardeshmukh, P. D., and B. J. Hoskins, 1988: The Generation of Global Rotational Flow by Steady Idealized Tropical Divergence. *J. Atmos. Sci.*, **45 (7)**, 1228–1251.

Serra, Y. L., G. N. Kiladis, and M. F. Cronin, 2008: Horizontal and vertical structure of easterly waves in the pacific itcz. *Journal of the Atmospheric Sciences*, **65 (4)**, 1266–1284, doi:10.1175/2007JAS2341.1, URL https://doi.org/10.1175/2007JAS2341.1, https://doi.org/10.1175/2007JAS2341.1.

Sikka, D. R., 1977: Some aspects of the life history, structure and movement of monsoon depressions. *pure and applied geophysics*, **115 (5)**, 1501–1529, doi:10.1007/BF00874421, URL http://dx.doi.org/10.1007/BF00874421.

Snyder, C., and R. S. Lindzen, 1991: Quasi-geostrophic wave-cisk in an unbounded baroclinic shear. *Journal of the Atmospheric Sciences*, **48 (1)**, 76–86, doi:10.1175/1520-0469(1991)048⟨0076:QGWCIA⟩2.0.CO;2, URL https://doi.org/10.1175/1520-0469(1991)048⟨0076:QGWCIA⟩2.0.CO;2, https://doi.org/10.1175/1520-0469(1991)048⟨0076:QGWCIA⟩2.0.CO;2.

Sobel, A., and E. Maloney, 2012: An idealized semi-empirical framework for modeling the Madden-Julian oscillation. *J. Atmos. Sci.*, **69 (5)**, 1691–1705.

Sobel, A., and E. Maloney, 2013: Moisture Modes and the Eastward Propagation of the MJO. *J. Atmos. Sci.*, **70 (1)**, 187–192.

Sobel, A. H., J. Nilsson, and L. M. Polvani, 2001: The Weak Temperature Gradient Approximation and Balanced Tropical Moisture Waves. *J. Atmos. Sci.*, **58 (23)**, 3650–3665.

Stano, G., T. N. Krishnamurti, T. S. V. V. Kumar, and A. Chakraborty, 2002: Hydrometeor structure of a composite monsoon depression using the trmm radar. *Tellus A*, **54 (4)**, 370–381, doi:10.1034/j.1600-0870.2002.01330.x, URL http://dx.doi.org/10.1034/j.1600-0870.2002.01330.x.

Subrahmanyam, D., M. K. Tandon, L. George, and S. K. Mishra, 1981: Role of barotropic mechanism in the development of a monsoon depression: A monex study. *pure and applied* *geophysics*, **119 (5)**, 901–912, doi:10.1007/BF00878958, URL http://dx.doi.org/10.1007/BF00878958.

Wolding, B. O., and E. D. Maloney, 2015: Objective Diagnostics and the Madden?Julian Oscillation. Part II: Application to Moist Static Energy and Moisture Budgets. *J. Climate*, **28 (19)**, 7786–7808, doi:10.1175/JCLI-D-14-00689.1, URL http://dx.doi.org/10.1175/JCLI-D-14-00689.1, http://dx.doi.org/10.1175/JCLI-D-14-00689.1.

Yoon, J.-H., and T.-C. Chen, 2005: Water vapor budget of the indian monsoon depression. *Tellus A*, **57 (5)**, 770–782, doi:10.1111/j.1600-0870.2005.00145.x, URL http://dx.doi.org/10.1111/j.1600-0870.2005.00145.x.

Yoon, J.-H., and W.-R. Huang, 2012: *02 Indian Monsoon Depression: Climatology and Variability*. InTech.

List of Tables

Variable	Symbol	Definition	Value/Units
Column latent energy anomaly	$\langle q' \rangle$	$\int_{100hPa}^{1000hPa} q' dp/g$	J m^{-2}
Precipitation anomaly	P'	$\langle q' \rangle \tau_c^{-1}$	W m^{-2}
Anomalous Streamfunction	ψ'		m^2 s^{-1}
Vorticity Anomaly	ζ'	$-\nabla^2 \psi'$	s^{-1}
Divergence Anomaly	D'	$\nabla \cdot \mathbf{V}'$	s^{-1}
Horizontal wind anomaly	$\mathbf{V}'$	(u', v')	m s^{-1}
Convective moisture adjustment timescale	τ_c	Eq. (1)	1 hour
Planetary vorticity at 20°N	f_0		5$\times$10^{-5} s^{-1}
Beta parameter	β	df/dy	2.2$\times$10^{-11} (m s)$^{-1}$
Thermal beta parameter	β_T	See Eq. (3)	0-1$\times$10^{-11}(m s)$^{-1}$
Specific heat of dry air at constant pressure	C_p		1004 J kg $^{-1}$ K^{-1}
Zonal wavenumber	k	$2\pi/\lambda_x$	m^{-1}
Meridional wavenumber	l	$2\pi/\lambda_y$	m^{-1}
Angular frequency	ω		s^{-1}
Mean gross dry stability	$\overline{M}_s$	$-\langle \Omega \partial \overline{S}/\partial p \rangle$	3.2 $\times$10^7 J m^{-2}
Mean gross moisture stratification	$\overline{M}_q$	$\langle \Omega \partial \overline{q}/\partial p \rangle$	2.7 $\times$10^7 J m^{-2}
Normalized gross moist stability	$\tilde{M}$	$(\overline{M}_s - \overline{M}_q)/\overline{M}_s$	0.15
Mean dry static energy	$\overline{S}$	$C_p\overline{T} + \overline{\Phi}$	J kg^{-1}
Mean barotropic wind	$\overline{u_0}$		5 m s^{-1}
Vertical velocity basis function	Ω	Eq. A7 in AK16	Pa
Wind / geopotential basis function	Λ	$-\partial \Omega/\partial p$	nondimensional
Phase speed of dry processes	c_{pd}^x	See Eq. (12b)	m s^{-1}
Phase speed of moist processes	c_{pm}^x	See Eq. (12c)	m s^{-1}
Total zonal phase speed	c_p^x	$\omega/k = c_{pm}^x + c_{pd}^x$	m s^{-1}
Zonal group velocity	c_g^x	$\partial \omega/\partial k$	m s^{-1}

TABLE 1. Basic variables and definitions used for Section 2.

List of Figures

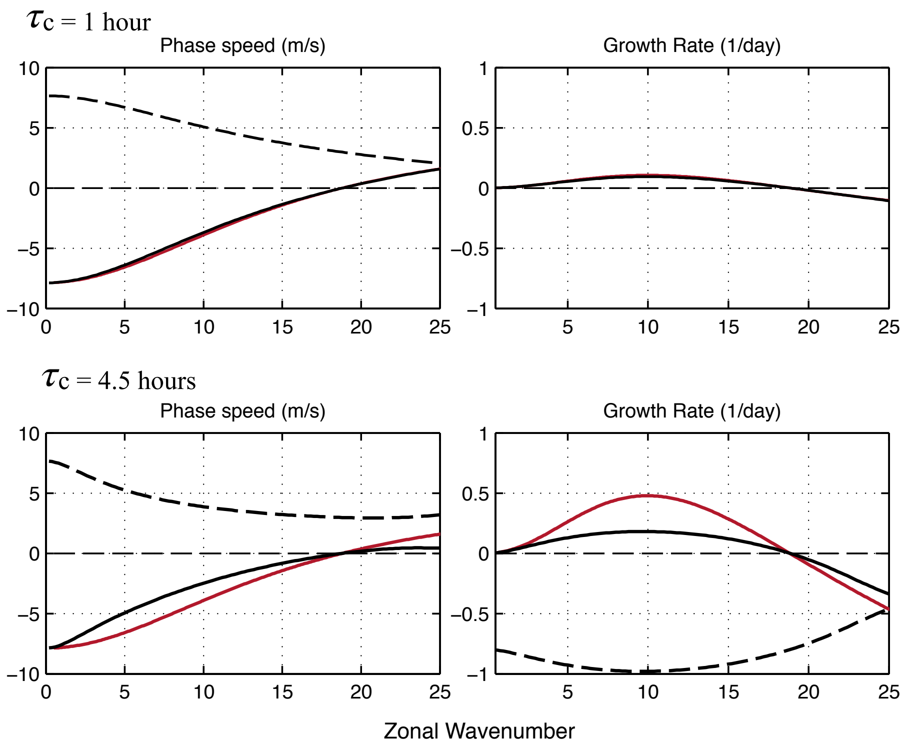

FIG. 1. Linear wave solutions of Eq. (9) (solid and dashed) for meridional wavenumber 15, $\overline{u_0} = 5$ m s^{-1}, $\tilde{M}$= 0.15, $\beta_T = 0.75 \times 10^{-11}$ m^{-1} s^{-1} , $\tau_c = 1$ (top) and 4.5 hours (bottom). The left column shows the phase speed and the right column shows the growth rate. The approximate solution (Eqs. 11 and 15) is shown as a red line.

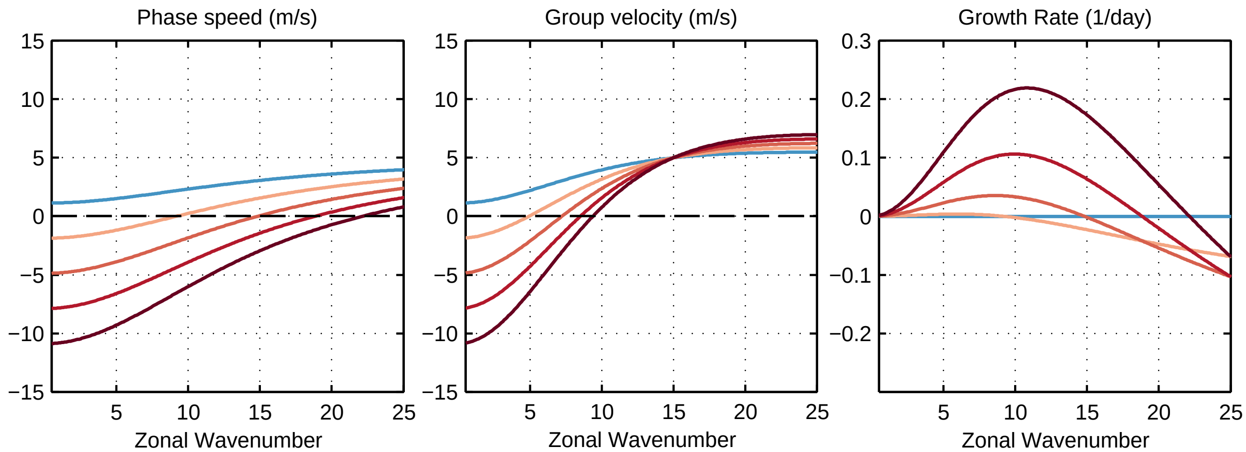

FIG. 2. Approximate phase speed, group velocity and growth rate for the monsoon low pressure system as obtained from Eqs. 11 and 15 for meridional wavenumber 15, $\overline{u_0} = 5$ m s^{-1}, $\tilde{M} = 0.15$, $\tau_c = 1$ hour, and values of β_T of 0, 0.25, 0.5, 0.75 and 1 $\times$ 10^{-11} m^{-1} s^{-1}. Redder shading indicates increasing values of β_T.

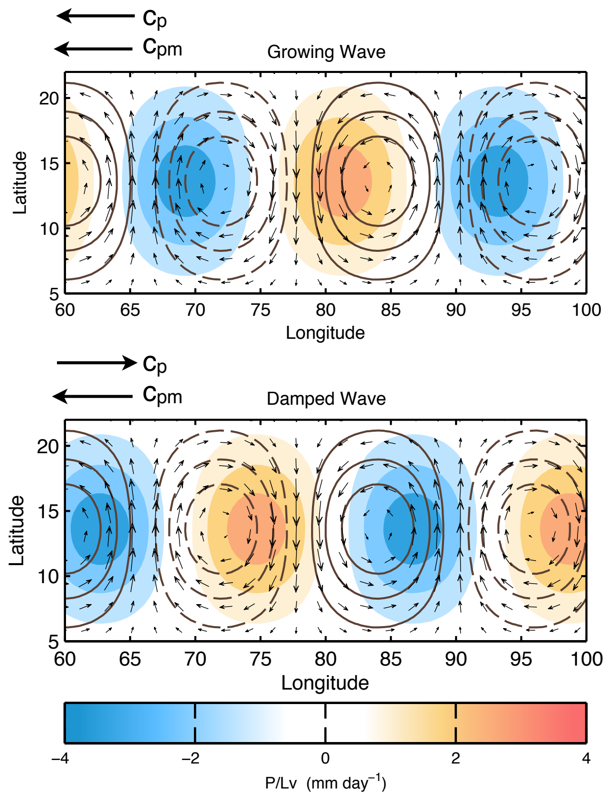

Fig. 3. Horizontal structure of a zonal wavenumbers 15 and meridionally-decaying structure in which (top) c_p^x and c_{pm}^x are westward and (bottom) c_p^x is eastward and c_{pm}^x is westward. Precipitation is shown as the shaded field, streamfunction is shown in contours and the horizontal wind as arrows. The largest arrows correspond to roughly 2 m s^{-1} . Contour interval is 0.25×10^6 m^2 s^{-1}. We use a value of β_T of 0.75×10^{-11} m^{-1} s^{-1} and A value of c_p^x of -6 m s^{-1} in the top panel, and 6 m s^{-1} in the bottom panel. A large value of τ_c of 18 hours is used to more clearly show how precipitation shifts in the growing and damped cases.

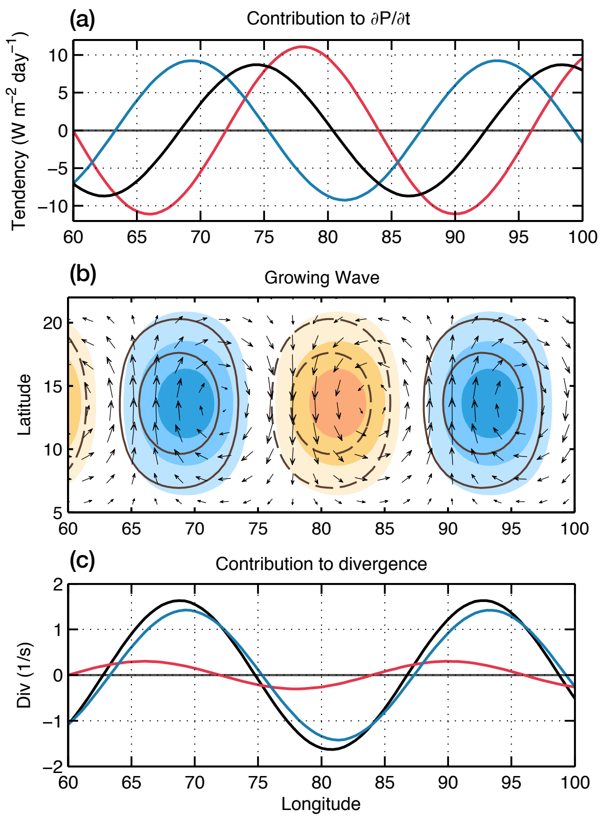

FIG. 4. (a) Contributions to the precipitation tendency ($\partial P/\partial t$, black line) by the adiabatic contribution from horizontal temperature advection (red line) and loss of moisture from precipitation (blue line). (b) As in the bottom panel of Fig. 3, but showing divergence as the contoured field . Contour interval $1\times\ 10^{-6}\ \mathrm{s}^{-1}$. (c) Total divergence (black line) and the adiabatic contribution from horizontal temperature advection (red) and the diabatic contribution from precipitation (blue). The red line, which describes quasi-geostrophic (QG) ascent, leads the precipitation anomalies. A large value of τ_c of 18 hours is used to more clearly show the phase shift between low-level convergence and precipitation.

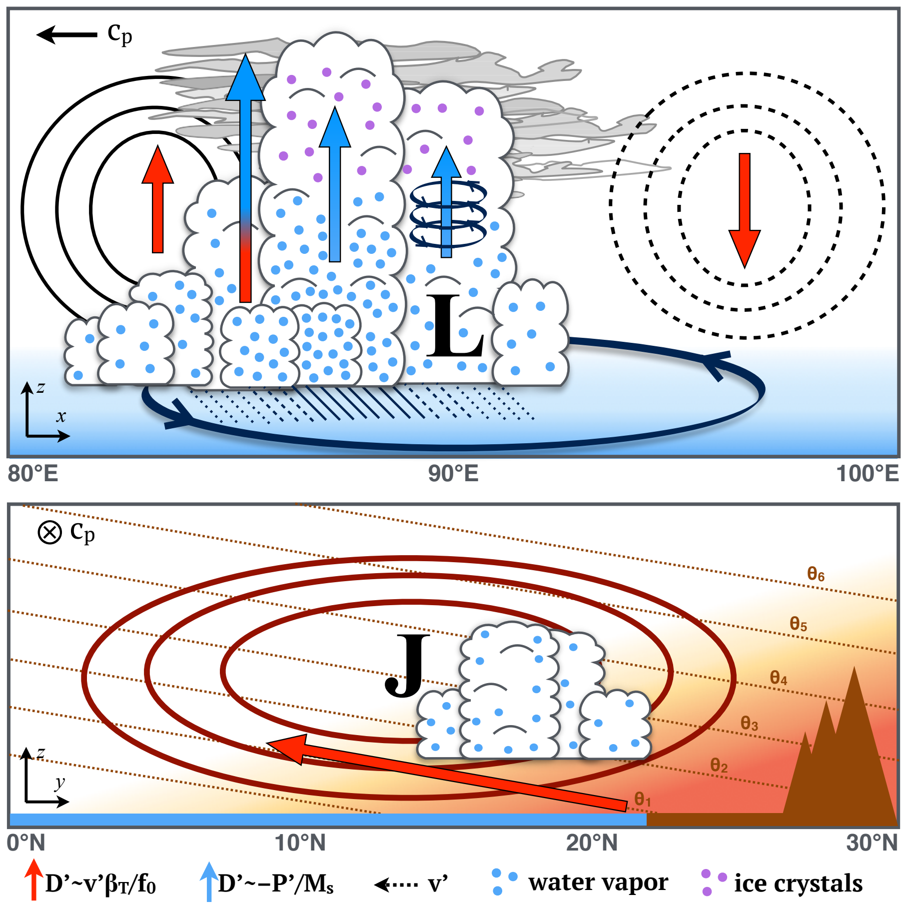

Fig. 5. Schematic describing the structure and propagation of a monsoon low pressure system. The top panel shows a longitude-height cross section while the bottom panel shows a latitude-height cross section corresponding to the left side of the top panel ($\sim$ 83°E). The anomalous northerly winds (solid contours in top panel, arrow in bottom panel) advect warm air from the Indian subcontinent. This warm air advection ascends along lines of constant potential temperature θ (isentropes, red vertical arrow), which moistens the free troposphere. This moistening creates favorable conditions for the subsequent development of deep convection (blue vertical arrow), which reaches a maximum amplitude to the west of the center of low pressure. The maximum in ascent (mixed blue and red arrow) is due to the sum of adiabatic ascent and convectively-driven ascent due to increased moisture. Deep convection induces the growth of the cyclone through vortex stretching (blue arrow with vortex rings). The boldface **L** depicts the center of the low pressure system and **J** represents the center of the low level westerly jet. Flow out of the page is depicted in solid and flow into the page is depicted in dashed. Water vapor content and ice crystals are depicted with circles, as in Janiga and Zhang (2016).